Role of intersublattice exchange interaction in ultrafast longitudinal and transverse magnetization dynamics in permalloy

A. Maghraoui, F. Fras, M. Vomir, Y. Brelet, V. Halté, J. Y. Bigot, and M. Barthelemy*

Université de Strasbourg, CNRS, Institut de Physique et Chimie des Matériaux de Strasbourg, UMR 7504, F-67000 Strasbourg, France

(Received 4 February 2021; revised 30 March 2023; accepted 30 March 2023; published 19 April 2023)

We report on element-specific measurements of ultrafast demagnetization and magnetization precession damping in permalloy thin films. Magnetization dynamics induced by an optical pump at 1.5 eV is probed simultaneously at the $M_{2,3}$ edges of Ni and Fe with high-order harmonics for moderate demagnetization rates (less than 50%). The role of the intersublattice exchange interaction in both longitudinal and transverse dynamics is analyzed with a Landau-Lifshitz-Bloch description of ferromagnetically coupled Fe and Ni sublattices. It is shown that the intersublattice exchange interaction governs the dissipation during demagnetization as well as precession damping of the magnetization vector.

DOI: 10.1103/PhysRevB.107.134424

I. INTRODUCTION

Ultrafast demagnetization of ferromagnets induced by femtosecond laser pulses [1–3] promises novel applications in data storage and processing technologies. Since its discovery, several microscopic mechanisms, including the spin-orbit interaction [4–6], Elliott-Yafet scattering-induced spins flips [7], nonthermal excitations [8,9], and superdiffusive [10,11] or ballistic spin transport, have been identified to play a key role, and their relative weight can be element dependent [12]. Depending on magnetic anisotropies, such transient modification of the effective magnetic field can trigger a coherent precession motion of the magnetization vector with a Gilbert damping [13] resulting from the dissipation of energy to an external bath. Those longitudinal and transverse relaxation processes set a natural limit on optical manipulation of magnetization from femtosecond to nanosecond timescales. If one aims to study the dynamics over such a large temporal scale, the Landau-Lifshitz-Bloch (LLB) model [14], in which the effective field contains the essential microscopic mechanisms, is well adapted. Among these mechanisms, the exchange interaction appears to be critical, but several aspects remain to be explored. In particular, in multiple-compound materials, the intersublattice exchange interaction plays a crucial role in the resulting global dynamics, acting as a spin momentum transfer between sublattices during the demagnetization [15]. Over the last decade, it has been investigated experimentally thanks to the chemical selectivity of the XUV resonant probe of core levels of transition metals (TMs) and rare earths (REs). Time-resolved x-ray magnetic circular dichroism (XMCD) [16–20] and time-resolved magneto-optical Kerr experiments (TMOKE) probed by tabletop high-order harmonics (HH) [21–29] have proven to offer a unique opportunity to study sublattice magnetization dynamics in alloyed ferromagnets. It is governed by dissipation and momentum transfer mechanisms in all-optical magnetization switching process [18–20]. In particular, the demagnetization of each sublattice in a binary alloy can be either accelerated or decelerated compared to the pure element demagnetization [21,22,24]. This effect is dependent on the value of elemental magnetic momenta and on the ferro- or antiferromagnetic nature of the exchange coupling [30,31]. The case of permalloy (Py) has attracted attention since various dynamical behaviors of sublattice magnetic momenta have been observed depending on the photon energy range of the probe. On the one hand, XMCD studies performed at $L_{2,3}$ edges have shown a faster demagnetization of Ni momenta compared to Fe [31]. This observation is supported by the strong effective exchange coupling sustained by Fe momenta in Py so that Ni sublattice momenta are subjected more to thermal dissipation [32]. On the other hand, HH TMOKE measurements show that during the early demagnetization of ferromagnetic Py, the momenta of Fe start to randomize before Ni momenta until a timescale of 10 fs, after which both sublattices relax together due to intersublattice exchange interaction (IEI) [24]. The origin of a stronger coupling of Fe spins to the electronic system compared to Ni remains unknown and deserves further exploration. In the present work, the magnetization dynamics of Fe and Ni sublattices of a 10 nm permalloy thin film is studied with chemical selectivity over a wide temporal range as a function of excitation density. A tabletop HH TMOKE configuration is used to measure both demagnetization and precession at the M edges of Fe and Ni. The role of strong intersublattice exchange interaction in longitudinal and transverse ultrafast magnetization dynamics is discussed for moderate demagnetization amplitudes.

II. EXPERIMENT

In our experiment, XUV pulses less than 10 fs are produced by HH generation in a Ne-filled gas cell driven by 795 nm, 3 mJ, 1 kHz, 25 fs laser pulses. The resulting XUV probe photon energies cover the 30–72 eV range and span the $M_{2,3}$

*Corresponding author: barthelemy@unistra.fr

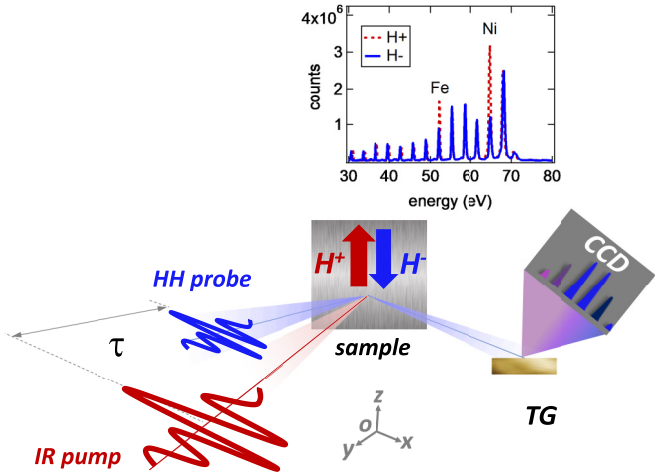

FIG. 1. Principle of the XUV probe IR pump transverse HH TMOKE experimental configuration with static magnetic field H along the z axis. TG: toroidal grating; CCD: charge coupled device camera. Inset: example of reflected spectra on Py for the antiparallel orientations of the applied magnetic field $\pm H$ (blue solid line and red dotted line, respectively).

edges of Fe and Ni centered, respectively, at 66 and 54 eV. Ultrafast demagnetization is induced by a 795 nm, 25 fs pump with variable fluence in a 10 nm thick $Ni_{80}Fe_{20}$ (Py) thin film with an in-plane anisotropy deposited on a crystalline Al_2O_3 substrate by ion beam sputtering.

Figure 1 illustrates the transverse time-resolved magneto-optical Kerr configuration used in this work. An external static magnetic field ($H = 450$ Oe) is applied to the sample along the transverse axis, i.e., along the z direction in Fig. 1 and perpendicular to the plane of incidence xOy of the p-polarized IR pump and VUV probe. The angle of incidence of the probe was set to 45° with respect to the sample normal in order to maximize the magnetic contrast obtained from spectrally resolved reflectivity measurements [21]. In the inset of Fig. 1, the reflected XUV probe spectra $I_{H^+}^{\text{stat}}$ and $I_{H^-}^{\text{stat}}$ are shown for two antiparallel orientations of the transverse magnetic field H. The maximum intensity difference between the two reflected spectra is seen at harmonics h_{45} (centered at 66 eV) and h_{35} (centered at 54 eV), corresponding to the M edges of Ni and Fe, respectively. Both spectra are further measured as a function of pump-probe delay by varying the optical path of the pump with a mechanical delay line.

III. ULTRAFAST DEMAGNETIZATION IN PERMALLOY PROBED AT THE M EDGES OF Ni AND Fe

We first consider the short timescale corresponding to the demagnetization process in permalloy. The elemental magnetization dynamics of Ni and Fe elements $m(q, \tau)$ measured as a function of the pump-probe delay τ is then integrated over each resonant qth harmonic:

$$\frac{\Delta m}{m}(q, \tau) = \frac{I_{H^+}^{\text{dyn}}(q, \tau) - I_{H^-}^{\text{dyn}}(q, \tau)}{I_{H^+}^{\text{stat}}(q) - I_{H^-}^{\text{stat}}(q)} \quad (1)$$

for $q = 45$ and $q = 35$, with $I_{H^\pm}^{\text{dyn}} = I_{H^\pm}^{\text{with}} - I_{H^\pm}^{\text{stat}}$, where $I_{H^\pm}^{\text{with}}$ is the intensity of the signal with pump and $I_{H^\pm}^{\text{stat}}$ is the intensity without pump. Figure 2 shows demagnetization $\frac{\Delta m}{m}(q, \tau)$ in Py at the $M_{2,3}$ edges of Fe ($\frac{\Delta m^{\text{Fe}}}{m^{\text{Fe}}}$) and Ni ($\frac{\Delta m^{\text{Ni}}}{m^{\text{Ni}}}$) integrated over harmonics h_{35} and h_{43}, respectively, for three increasing pump fluences. Ni and Fe sublattices appear to demagnetize simultaneously. The demagnetization amplitude of both sublattices increases from 25% to 40%. Long exposure above 40% demagnetization resulted in damaging the sample and prevented the realization of a long scan. In contrast to Ref. [24], no reproducible delay between the two sublattice demagnetizations is observed with our pump duration of 25 fs. A possible explanation could be a slight variation of the intersublattice exchange interaction (sample dependent due to the change in crystallinity or grating vs alloy) that may induce a change in the temporal shift value. Moreover, the different conditions of HH generation could lead to a different time duration of our probe, resulting in a lower temporal resolution, or a delay between h_{35} and h_{45} due to a possible chirp.

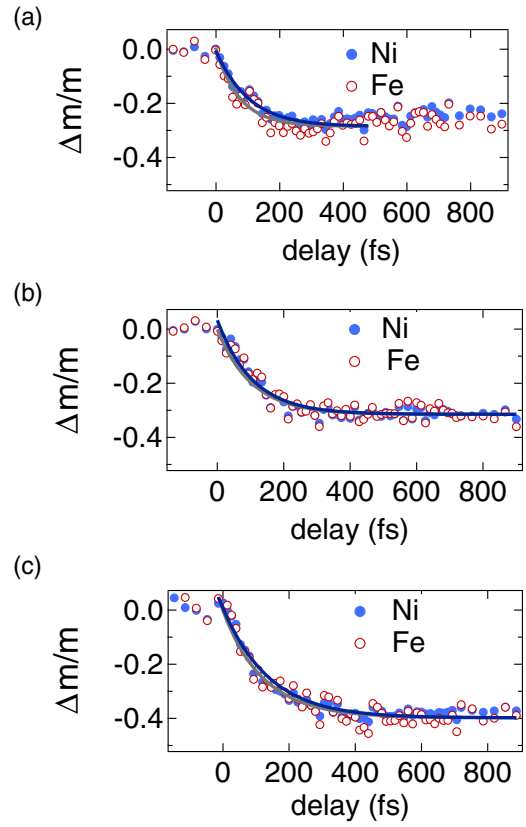

FIG. 2. Demagnetization dynamics in permalloy probed at the Ni (solid blue dots) and Fe (open red dots) M edges and fits (gray lines: Fe, blue lines: Ni) for incident pump fluences of (a) 2.5 mJ/cm^2, (b) 3.8 mJ/cm^2, and (c) 4.7 mJ/cm^2.

The framework of analysis and data fitting is described in the following, and details of the linearized LLB are presented. This approach is based on knowledge of the laser-induced temperature of the system. In order to define such a laser-induced temperature, let us first explore the demagnetization amplitude behavior with incident pump fluence.

The demagnetization amplitude of Ni and Fe in permalloy with respect to the pump fluence is plotted in Fig. 3.

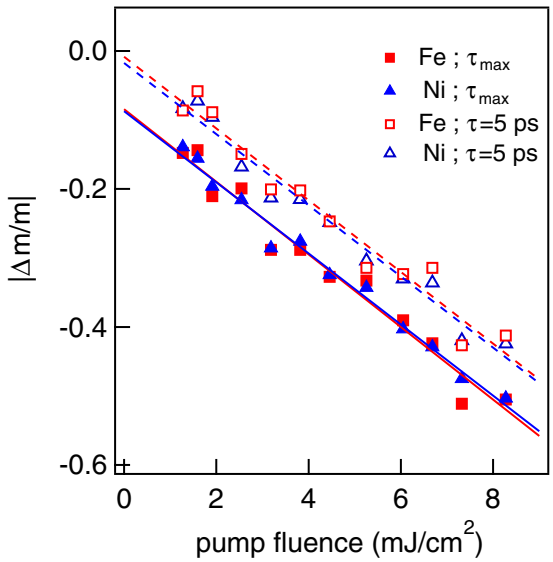

FIG. 3. Demagnetization amplitudes measured at M edges of Ni and Fe in Py as a function of incident pump fluence for maximum demagnetization (solid symbols) and at a 5 ps pump-probe delay (open symbols).

For each point, two delays have been chosen. The first delay corresponds to the maximal demagnetization level (the corresponding time delay range is 300–500 fs from low to large pump fluences); the second delay is fixed at 5 ps and corresponds to a thermal quasiequilibrium between electrons and lattice baths (remagnetization). Within the fluence range of this experiment the demagnetization amplitude is always found to be identical for both sublattices. Moreover, up to 40% demagnetization given by the damage threshold of our sample, a linear increase in demagnetization amplitude with the pump fluence is observed, with the same slope for both delays. Such linear behavior can be attributed to a coupling with a thermalized bath [2], characterized by an energy of $k_B T$, heated by the laser pulse. The vertical offset between the two curves arises from a picosecond remagnetization originating from a fast cooldown of the spin bath through coupling with the lattice [33]. In the LLB approach, it can be described as a temperature step between the maximal bath temperature (demagnetization) and the cooldown of the bath due to coupling with the lattice (remagnetization). One can notice that the linear fits labeled maximum do not cross the zero variation at zero fluence. At a delay of 5 ps a slight deviation from zero is also observed. This range of fluence is either difficult to access experimentally or usually not considered. A hypothesis to explain such a behavior is a change in the regime of interaction, at the origin of the demagnetization or remagnetization processes, with pump fluence. This could lead to a different power-dependent law in the range of very low fluences, but this aspect goes beyond the scope of the present work. After thermalization of electrons, the temperature-dependent normalized magnetization can be approximated with a molecular field model as

$$\mathbf{m}^{\epsilon}(T) = \left(1 - \frac{T}{T_C}\right)^{\kappa^{\epsilon}}, \tag{2}$$

where T_C is the Curie temperature and κ^{ϵ} is the critical exponent. In the following, the maximum amplitude of demagnetization in our experiments is used to evaluate the laser-induced spin temperature T that is related to the amplitude of fluctuations to which the spins are submitted [34] in the 300–500 fs temporal range. As in Ref. [32], in our approach at short timescales, only the demagnetization process is considered, justified by a slower rate (a few picoseconds in our case [7,33]) of the remagnetization process. The magnetic system can be considered to be initially in thermal equilibrium at a temperature of $T_i = 300$ K; then for $t = 0$ the bath temperature is instantaneously changed to T_f. Thus, the magnetization of the two sublattices will evolve towards a new thermal equilibrium value given by T_f. Therefore, in this approach, the equivalent spin temperature is defined at the maximum of demagnetization. By taking a Curie-Weiss law ($\kappa = 1/2$) and $T_C = 850$ K in $Ni_{80}Fe_{20}$, the temperature range can be calibrated. In Fig. 3, the evaluated spin temperature T ranges from 300 to 600 K, and the maximum demagnetization amplitudes in Fig. 2 correspond to $T/T_C = 0.35$, 0.43, and 0.52.

We now analyze our experimental data in the frame of the linearized LLB model. It considers an ensemble of rigid spins submitted to exchange interaction and coupled to a thermal bath, corresponding to either charges or phonons at the origin of dissipation [34–38]. It gives a consistent approach that encompasses a broad temporal scale from femtoseconds to nanoseconds, during which spin flips and the magnetization precession takes place. By isolating the longitudinal contribution to magnetization dynamics at short timescales, it can be used to simulate ultrafast demagnetization in TM-RE compounds. This method was first applied to ferrimagnets, which are known for their high potential for all-optical switching [34], and was used more recently to better understand the role of IEI in ferromagnetic TM alloys [32]. In particular, this model allows us to decipher quantitatively the role played by both the IEI and intrinsic dissipation of each sublattice's magnetization in the observed dynamics. Fe and Ni momentum dynamics in permalloy are described with the following first-order coupled rate equation:

$$\begin{pmatrix} \dot{\mathbf{m}}^{\mathrm{Fe}} \\ \dot{\mathbf{m}}^{\mathrm{Ni}} \end{pmatrix} = \mathcal{A}_{\parallel} \begin{pmatrix} \mathbf{m}^{\mathrm{Fe}} \\ \mathbf{m}^{\mathrm{Ni}} \end{pmatrix} = \begin{pmatrix} -\Gamma_{\mathrm{FeFe}} & \Gamma_{\mathrm{FeNi}} \\ \Gamma_{\mathrm{NiFe}} & -\Gamma_{\mathrm{NiNi}} \end{pmatrix} \begin{pmatrix} \mathbf{m}^{\mathrm{Fe}} \\ \mathbf{m}^{\mathrm{Ni}} \end{pmatrix}, \tag{3}$$

where the matrix $\mathcal{A}_{\parallel}$ drives the dynamics. Its elements can be written as a function of micromagnetic parameters [32]:

$$\Gamma_{\mathrm{FeFe}} = \frac{1}{\tau^{\mathrm{Fe}}_{\mathrm{intra}}} + \frac{\chi^{\mathrm{Ni}}_{\parallel}}{\chi^{\mathrm{Fe}}_{\parallel}} \frac{1}{\tau^{\mathrm{FeNi}}_{\mathrm{exch}}}, \tag{4}$$

$$\Gamma_{\mathrm{FeNi}} = \frac{1}{\tau^{\mathrm{FeNi}}_{\mathrm{exch}}}, \tag{5}$$

$$\Gamma_{\mathrm{NiFe}} = \frac{1}{\tau^{\mathrm{NiFe}}_{\mathrm{exch}}}, \tag{6}$$

$$\Gamma_{\mathrm{NiNi}} = \frac{1}{\tau^{\mathrm{Ni}}_{\mathrm{intra}}} + \frac{\chi^{\mathrm{Fe}}_{\parallel}}{\chi^{\mathrm{Ni}}_{\parallel}} \frac{1}{\tau^{\mathrm{NiFe}}_{\mathrm{exch}}}. \tag{7}$$

In this basis, the elements of $\mathcal{A}_{\parallel}$ contain two contributions to longitudinal damping. The first one corresponds to intra-

sublattice demagnetization τ_{intra}:

$$\frac{1}{\tau_{\text{intra}}^{\text{Fe,Ni}}} = \frac{\gamma^{\text{Fe,Ni}}\alpha_{\parallel}^{\text{Fe,Ni}}(T)}{\chi_{\parallel}^{\text{Fe,Ni}}(T)}, \tag{8}$$

where $\alpha_{\parallel}^{\text{Fe,Ni}}$ is longitudinal damping and $\chi_{\parallel}^{\text{Fe,Ni}}$ is the effective magnetic susceptibility, both of which are element- and temperature-dependent quantities. $\gamma^{\text{Fe,Ni}}$ corresponds to the gyromagnetic ratio of each element. The second one is the intersublattice exchange-mediated demagnetization:

$$\frac{1}{\tau_{\text{exch}}^{\text{FeNi,NiFe}}} = \frac{\gamma^{\text{Fe,Ni}}\alpha_{\parallel}^{\text{Fe,Ni}}(T)J_{\text{FeNi,NiFe}}}{\mu^{\text{Fe,Ni}}}, \tag{9}$$

where $J_{\text{FeNi}} = J_{\text{NiFe}}$ is the IEI constant and $\mu_{\text{Fe,Ni}}$ is the atomic magnetic momentum.

Finally, diagonal terms of $\mathcal{A}_{\parallel}$, $-\Gamma_{\text{FeFe}}$ and $-\Gamma_{\text{NiNi}}$, correspond to a dissipation of magnetic momenta in each sublattice. The IEI can affect this dissipation rate, as reflected by the second term in Eqs. (4) and (7), but also leads to an exchange of momentum translated by the nondiagonal terms Γ_{NiFe} and Γ_{FeNi}, leading to an exchange of momentum between sublattices. It should be underlined that, in this approach, the overall flow of momentum, mediated by the IEI, is element dependent and weighted by the magnetic susceptibility ratio.

The differential system (3) can be easily solved in the eigenbasis after diagonalization of $\mathcal{A}_{\parallel}$:

$$\mathcal{A}_{\parallel} = \begin{pmatrix} \Gamma^{+} & 0 \\ 0 & \Gamma^{-} \end{pmatrix}, \tag{10}$$

where the two eigenvalues $\Gamma^{\pm} = 1/\tau^{\pm}$ can be written as

$$\Gamma^{\pm} = \tfrac{1}{2}[\Gamma_{\text{FeFe}} + \Gamma_{\text{NiNi}} \pm \sqrt{(\Gamma_{\text{FeFe}} - \Gamma_{\text{NiNi}})^2 + 4\Gamma_{\text{FeNi}}\Gamma_{\text{NiFe}}}]. \tag{11}$$

Finally, the measured sublattice magnetization dynamics can be expressed as a linear combination of the differential system solutions:

$$\frac{\Delta\mathbf{m}^{\text{Fe}}}{\text{m}^{\text{Fe}}} = A^{\text{Fe}}\exp\left(-\frac{t}{\tau^{+}}\right) + B^{\text{Fe}}\exp\left(-\frac{t}{\tau^{-}}\right), \tag{12}$$

$$\frac{\Delta\mathbf{m}^{\text{Ni}}}{\text{m}^{\text{Ni}}} = A^{\text{Ni}}\exp\left(-\frac{t}{\tau^{+}}\right) + B^{\text{Ni}}\exp\left(-\frac{t}{\tau^{-}}\right), \tag{13}$$

where the coefficients A^{Fe}, B^{Fe}, A^{Ni}, and B^{Ni} depend on the eigenvector components $x^{\pm} = \Gamma_{\text{FeNi}}/(\Gamma_{\text{FeFe}} - 1/\tau^{\pm})$ as follows:

$$A^{\text{Fe}} = \Delta m_0^{\text{Fe}}\frac{x^{+}}{(x^{-} - x^{+})}\left(\frac{\Delta m_0^{\text{Ni}}}{\Delta m_0^{\text{Fe}}}x^{-} - 1\right), \tag{14}$$

$$B^{\text{Fe}} = \Delta m_0^{\text{Fe}}\frac{x^{+}}{(x^{-} - x^{+})}\left(1 - \frac{\Delta m_0^{\text{Ni}}}{\Delta m_0^{\text{Fe}}}x^{+}\right), \tag{15}$$

$$A^{\text{Ni}} = \Delta m_0^{\text{Fe}}\frac{1}{(x^{-} - x^{+})}\left(\frac{\Delta m_0^{\text{Ni}}}{\Delta m_0^{\text{Fe}}}x^{-} - 1\right), \tag{16}$$

$$B^{\text{Ni}} = \Delta m_0^{\text{Fe}}\frac{1}{(x^{-} - x^{+})}\left(1 - \frac{\Delta m_0^{\text{Ni}}}{\Delta m_0^{\text{Fe}}}x^{+}\right), \tag{17}$$

with Δm_0^{Fe} and Δm_0^{Ni} corresponding to the maximum amplitude of demagnetization. It is important to note that $\tau^{\pm}$ corresponds to $\tau^{\text{Fe,Ni}}$ only in the very low temperature range,

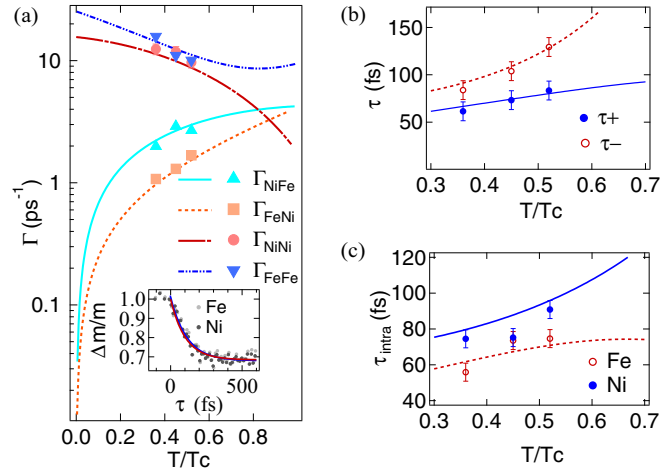

FIG. 4. Comparison of theoretical data from [32] (lines) and experimental values (symbols). (a) LLB matrix components for pump energy densities of $T/T_C = 0.35$, 0.42, and 0.52 for experiment (symbols) and theory (lines). Inset: example of M edge demagnetization global fitting (lines), giving rise to the LLB matrix element for 3.8 mJ/cm^2 pump fluence. (b) Characteristic times of M edge magnetization dynamics τ^{+} (open red circles) and τ^{-} (solid blue dots) and (c) $\tau_{\text{intra}}^{\text{Ni}}$ (solid blue dots) and $\tau_{\text{intra}}^{\text{Fe}}$ (open red circles) retrieved from experiment compared with theoretical values as a function of temperature.

where $1/\tau_{\text{exch}}^{\text{NiFe}}$ and $1/\tau_{\text{exch}}^{\text{FeNi}}$ are negligible. In the range of temperatures explored in our experiment, due to IEI, the dynamics of each sublattice is a clear biexponential decay, as shown in Eqs. (12) and (13), where the demagnetization time is a composition of τ^{-} and τ^{+}. Having in hand the T/T_C values equivalent to pump fluences from the amplitudes of demagnetization of our experiment, we can analyze our results in the frame of the linearized LLB model. As shown earlier, the pump fluence range used in our experiments corresponds to an intermediate temperature range, $0.35 < T/T_C < 0.52$. Figure 4 shows a comparison between theoretical values obtained from the multiscale LLB approach in [32] and our experimental ones for the subsequent components of the LLB matrix $\mathcal{A}_{\parallel}$ [Fig. 4(a)] and $\tau^{+} = 1/\Gamma^{+}$ and $\tau^{-} = 1/\Gamma^{-}$ [Fig. 4(b)], which are the characteristic times of the biexponential solutions of differential equations that govern the two sublattices' dynamics. For each pump fluence and corresponding laser-induced temperature, a global fitting procedure is used simultaneously for both Fe and Ni M edge demagnetization measurements to retrieve the $\mathcal{A}_{\parallel}$ matrix elements plotted as symbols in Fig. 4(a). From those values, A^{ϵ}, B^{ϵ}, and $\tau^{\pm}$ can be calculated and injected in Eqs. (12) and (13). An example of the corresponding $\Delta\mathbf{m}^{\text{Fe}}/m^{\text{Fe}}$ and $\Delta\mathbf{m}^{\text{Ni}}/m^{\text{Ni}}$ curves is plotted as lines in the inset of Fig. 4(a). It reproduces very well the observed demagnetization dynamics in Py measured at the M edges of Fe and Ni sublattices. Moreover, very good agreement is obtained between the theoretically predicted values of the $\mathcal{A}_{\parallel}$ elements and those extracted from our experiment fits (shown as lines in Fig. 2). The nondiagonal elements of $\mathcal{A}_{\parallel}$ retrieved from experiments confirm that IEI-mediated dissipation is much stronger for the Ni sublattice compared to Fe ($\Gamma_{\text{NiFe}} > \Gamma_{\text{FeNi}}$). Indeed, the IEI-induced

modifications of the two sublattice dynamics are not the same due to the element dependence of $\Gamma_{\mathrm{FeNi,NiFe}}$ (via the element dependence of $\alpha_{\parallel}^{\mathrm{Fe,Ni}}$, $\mu^{\mathrm{Fe,Ni}}$, and $\gamma^{\mathrm{Fe,Ni}}$). Interestingly, the temperature step model associated with the linearized LLB model works well to fit our measurements. A possible explanation could be that (i) thermalization of charge is faster than demagnetization (less than tens of femtoseconds), as observed in nickel thin films in [5], or (ii) only the energy step of the electrons drives the dynamics and thus athermal electron dynamics do not contribute significantly to demagnetization dynamics here. In order to discuss the intrasublattice dissipation (without the contribution of IEI), we extract the intrasublattice demagnetization time from our measurements, as shown in Fig. 4(c). It is deduced from the experimentally retrieved values of $\mathcal{A}_{\parallel}$ matrix elements and from Eqs. (4) and (7) by taking a constant ratio of magnetic susceptibilities $\chi_{\parallel}^{\mathrm{Fe}}/\chi_{\parallel}^{\mathrm{Ni}} = 2$ (valid in the intermediate temperature range, i.e., $T/T_C < 0.5$ [32]). Up to $T/T_C = 0.52$, $\tau_{\mathrm{intra}}^{\mathrm{Ni}} - \tau_{\mathrm{intra}}^{\mathrm{Fe}} < 15$ fs. Without IEI [Fig. 4(c)], the Fe sublattice undergoes stronger dissipation. This disparity between intrasublattice dissipations is compensated by strong IEI, leading to a common dynamics of both sublattices [Fig. 4(b)]. The above approach has the advantage of explaining the observed dynamics strongly influenced by IEI. It shows that IEI-mediated dissipation does not necessarily have the same weight in each sublattice. Moreover, the rate of intrasublattice dissipation mediated by IEI is related to the sublattice magnetic susceptibility ratio, which is almost constant for moderate laser-induced temperature and diverges close to T_C. Let us discuss this substantial difference from the definition of a unique exchange time less than 10 fs observed in a previous work. Indeed, in the pioneering study proposed by Mathias *et al.* [24], an exchange interaction time is introduced as a constant parameter that couples the two subsystems' magnetization dynamics. The key differences are based on the following points. In Ref. [24], the process of IEI is considered in a conservative manner with equal rates of magnetic momentum transfer between the two sublattices. The exchange interaction times are equal for both sublattices and independent of fluence. Finally, the data analysis, performed in this framework, imposes a strong difference between τ_{Fe} and τ_{Ni} (see the supplementary information in [24]). The LLB-based approach is fundamentally different since it considers the effect of IEI as related to the conservative transfer of momentum between sublattices and also to dissipation [Eqs. (4)–(7)]. Second, with the LLB approach, these contributions are both found to be element and temperature dependent [Eq. (9)] due to longitudinal damping and magnetic susceptibilities. The outcome analysis allows us to retrieve the intrasublattice demagnetization times: between 80 and 100 fs for both Fe and Ni, which is consistent with earlier observations [7,39].

IV. ULTRAFAST MAGNETIZATION PRECESSION AND DAMPING IN PERMALLOY PROBED AT THE *M* EDGES OF Ni AND Fe

We have shown the influence of the intersublattice exchange interaction on longitudinal magnetization dynamics occurring on a timescale of hundreds of femtoseconds. We now address the question of how IEI affects the damping

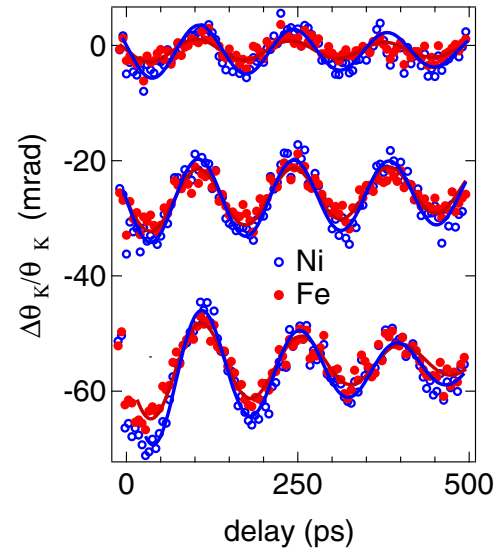

FIG. 5. Precession measurements in permalloy probed with high-order harmonics. Fe *M* edge (solid red dots) and Ni *M* edge (open blue circles) magnetization dynamics of precession in permalloy as a function of incident pump laser fluence, increasing from top to bottom: 1.5, 2.5, and 4 mJ/cm^2.

of the transverse motion of the magnetization vector, i.e., precessional motion over hundreds of picoseconds. In the following, the IR pump, XUV probe TMOKE experiments are performed in a 500 ps temporal range with a tilt of the external magnetic field axis of 10° with respect to the sample plane. This configuration allows for transverse projection measurement of the magnetization precession at the $M_{2,3}$ edges of Fe and Ni simultaneously. Both Kerr rotation signals $\Delta\theta_K/\theta_K$ integrated over h_{35} (Fe) and h_{43} (Ni) have been fitted using the following fitting function: $A^{\mathrm{Ni,Fe}}\sin(2\pi/T_{\mathrm{pr}}^{\mathrm{Ni,Fe}}t + \phi^{\mathrm{Ni,Fe}})\exp(-t/T_{\mathrm{d}}^{\mathrm{Ni,Fe}}) + B^{\mathrm{Ni,Fe}}$, where $A^{\mathrm{Ni,Fe}}$, $T_{pr}^{\mathrm{Ni,Fe}}$, $\phi^{\mathrm{Ni,Fe}}$, and $T_{\mathrm{d}}^{\mathrm{Ni,Fe}}$ are, respectively, the precession amplitudes, periods, phases, and damping times of each sublattice. $B^{\mathrm{Ni,Fe}}$ is an offset that corresponds to magnetization recovery with a long time delay compared to the temporal window of our measurements.

As seen in Fig. 5, the Ni and Fe momentum precessions are measured selectively in $Ni_{80}Fe_{20}$ for three incident pump fluences corresponding to an initial 25% to 35% of laser-induced demagnetization. The precession motion at the Ni edge has a slightly higher amplitude. While the precession signals are increased in amplitude with pump fluence, Fe and Ni momenta still precess in phase. Within the range of pump fluences used, the precession period stays quasiconstant, $T_{\mathrm{pr}}^{\mathrm{Ni,Fe}} \sim 150$ ps. The damping time remains identical for both sublattices. It is found to be about 2 ns for the intermediate fluence and is decreased down to 300 ps at the highest fluence. For the lowest fluence the damping time is difficult to extract within our temporal window and has a lower signal-to-noise ratio. It is estimated to be higher than 2 ns. Such an increase in damping can be explained by the increase in the phonon-mediated spin-flip rate with increasing fluence. Indeed, the generated phonon density increases with pump fluence. Phonons cause crystal field fluctuations, modulating the magnetocrystalline

anisotropy and leading to random torques on the spins. We now analyze the Gilbert damping in the frame of the Landau-Lifshitz-Gilbert equation. On the timescale of the transverse damping (three orders of magnitude longer than the short timescale of ultrafast demagnetization), the precession motion of the magnetization of two coupled sublattices ϵ and δ can be written for $\mathbf{m}^{\epsilon,\delta}$ as [40]

$$\frac{\dot{\mathbf{m}}^{\epsilon}}{\gamma^{\epsilon}} = -(\mathbf{m}^{\epsilon} \times \mathbf{H}'_{\epsilon}) - \alpha^{\epsilon}[\mathbf{m}^{\epsilon} \times (\mathbf{m}^{\epsilon} \times \mathbf{H}'_{\epsilon})] + A_{\epsilon\delta} m_s^{\delta}\{(\mathbf{m}^{\epsilon} \times \mathbf{m}^{\delta}) + \alpha^{\epsilon} A_{\epsilon\delta} m_s^{\delta}[\mathbf{m}^{\epsilon} \times (\mathbf{m}^{\epsilon} \times \mathbf{m}^{\delta})]\}, \tag{18}$$

with m_s^{δ} being the saturation magnetization of the second sublattice δ. The first line of Eq. (18) corresponds to the precession of magnetization and damping related to the effective field $\mathbf{H}'_{\epsilon} = \mathbf{H}_0 + \mathbf{H}_{\text{anis}}$, where γ^{ϵ} is the gyromagnetic ratio, α^{ϵ} is the Gilbert damping, and $\mathbf{H}_0$ and $\mathbf{H}_{\text{anis}}$ are the applied and anisotropy fields. The second line corresponds to the coupling of the precession motion and damping via IEI $J_{\epsilon\delta}$ between sublattices ϵ and δ. It corresponds to a contribution to the effective field $\mathbf{H}''_{\epsilon} = -A_{\epsilon\delta} m_s^{\delta} \mathbf{n}^{\delta}$ of the second sublattice δ on the first sublattice ϵ. The exchange stiffness parameter is defined by $A_{\epsilon\delta} = J_{\epsilon\delta}/\mu_{\delta}\mu_{\epsilon}$.

Note that when $A_{\epsilon\delta}$ is lower than other elemental effective field contributions, the two sublattices precess independently. In our case, when $A_{\epsilon\delta}$ dominates, the resulting motion corresponds to a single coupled precession motion. The corresponding Gilbert damping can be evaluated from the damping time T_{d}^{Py} as a single value for each fluence. Considering a circular precession motion with small angles, we have

$$\alpha^{\text{Py}} = 1/\left(T_{\text{d}}^{\text{Py}} \omega^{\text{Py}}\right), \tag{19}$$

with $\omega^{\text{Py}} = 2\pi/T_{pr}$ being the precession pulsation. From our measurements in Py at the M edges of Ni and Fe (Fig. 5) and by taking $m_{\text{s}}^{\text{Py}} = 8.4\ 10^6 \text{A m}^{-1}$, we have $\alpha^{\text{Ni,Py}} \sim \alpha^{\text{Fe,Py}} \leqslant 0.012$ for the first two fluences and $\alpha^{\text{Ni,Py}} \sim \alpha^{\text{Fe,Py}} = 0.079$ for the maximal fluence. Moreover, in a strongly exchange coupled alloy, the Gilbert damping can be estimated as an effective damping from pure element parameters [41]:

$$\alpha_{\text{eff}}^{\text{Py}} = \frac{m_s^{\text{Fe}} \gamma^{\text{Ni}} \alpha^{\text{Fe}} + m_s^{\text{Ni}} \gamma^{\text{Fe}} \alpha^{\text{Ni}}}{m_s^{\text{Fe}} \gamma^{\text{Ni}} + m_s^{\text{Ni}} \gamma^{\text{Fe}}}, \tag{20}$$

where α^i (i = Ni, Fe) is the pure element damping. To compare the estimated value of damping α^{Py} from the HH generation experiment to the one that is a composition of pure elements $\alpha_{\text{eff}}^{\text{Py}}$, we have performed precession measurements on two 10 nm thick films of pure Ni and pure Fe using a TMOKE configuration with 25 fs, 800 nm pulses. The measured precession damping times $T_d^{\text{Ni, pure}}$ and $T_d^{\text{Fe,pure}}$ at a fixed initial demagnetization of 20% allow us to retrieve the corresponding Gilbert dampings $\alpha^{\text{Ni,pure}}$ and $\alpha^{\text{Fe,pure}}$ by using Eq. (19). By taking $m_{\text{s}}^{\text{Fe,pure}} = 1.72\ 10^6 \text{A m}^{-1}$ and $m_{\text{s}}^{\text{Ni,pure}} = 4.85\ 10^6 \text{A m}^{-1}$, the following Gilbert damping values are obtained for pure thin films: $\alpha^{\text{Ni,pure}} = 0.05$ and $\alpha^{\text{Fe,pure}} = 0.016$. The effective damping in Py as a composition of pure element damping obtained with Eq. (20), $\alpha_{\text{eff}}^{\text{Py}} = 0.041$ (with $\gamma^{\text{Fe}} = 2.12\ 10^5 \text{ m s}^{-1}\text{A}^{-1}$ and $\gamma^{\text{Ni}} = 2.03\ 10^5 \text{ m s}^{-1}\text{A}^{-1}$), is in good agreement with values found with Eq. (19). Finally, we note that the common Gilbert damping value measured at both Fe and Ni M edges in Py is close to the highest pure Ni value. This indicates that the dissipation of precession is dominated by the Ni sublattice contribution. This could be attributed to the higher spin-orbit coupling in Ni compared to Fe, leading to a higher spin lattice dissipative contribution [12,13].

V. CONCLUSION

In this work, the magnetization dynamics in Py induced by a 1.5 eV femtosecond pump pulse and probed by HH was investigated with chemical selectivity in Ni and Fe sublattices over a wide temporal scale. The role played by the IEI in the sublattice damping and precession was explored in the intermediate spin temperature range. First, we showed that demagnetization dynamics measured at the M edge of each Fe and Ni sublattice of permalloy is well reproduced in the LLB framework. The pump fluence dependent dynamics of each sublattice is characterized by double exponential decay with characteristics times τ_+ and τ_-, relying on both elemental susceptibilities and longitudinal damping. This approach allows us to distinguish two contributions to the demagnetization time measured at the M edges of each sublattice: the first one corresponds to intrasublattice dissipation governed by longitudinal damping and magnetic susceptibilities; the second one is the IEI-mediated dissipation responsible for the strongly coupled response observed in this study. An interesting prospect could be to study magnetization dynamics beyond this range of excitation densities, where the two sublattices are expected to show different dynamics, as predicted by the LLB model.

Second, we showed that not only the longitudinal magnetization dynamics of each sublattice but also the magnetization vector orientation through precession and transverse damping is dominated by IEI. The strong IEI drives the two sublattices to share a single precession mode whose the damping is a composition of pure element damping. Fundamentally, those results improve the understanding of the role of the exchange interaction in ultrafast magnetization dynamics. Moreover, they open prospects in the design of new complex magnetic materials for data processing, such as alloys and multilayer ferromagnets.

ACKNOWLEDGMENTS

The authors would like to thank G. Versini for sample preparation and G. Dekyndt, N. Beyer, G. Versini, M. Albrecht, and J. Faerber for technical assistance. This work has been supported by the European Research Council ("Atomag" project ERC-2009-AdG-20090325, No. 247452), and Agence Nationale de la Recherche ("Union" project, Grant No. ANR-10-EQPX-52).

[1] E. Beaurepaire, J. C. Merle, A. Daunois, and J. Y. Bigot, Phys. Rev. Lett. **76**, 4250 (1996).

[2] J. Hohlfeld, E. Matthias, R. Knorren, and K. H. Bennemann, Phys. Rev. Lett. **78**, 4861 (1997).

[3] M. Aeschlimann, M. Bauer, S. Pawlik, W. Weber, R. Burgermeister, D. Oberli, and H. C. Siegmann, Phys. Rev. Lett. **79**, 5158 (1997).

[4] G. P. Zhang and W. Hubner, Phys. Rev. Lett. **85**, 3025 (2000).

[5] J. Y. Bigot, M. Vomir, and E. Beaurepaire, Nat. Phys. **5**, 515 (2009).

[6] K. Krieger, J. K. Dewhurst, P. Elliott, S. Sharma, and E. K. U. Gross, J. Chem. Theory Comput. **11**, 4870 (2015).

[7] B. Koopmans, G. Malinowski, F DallaLonga, D. Steiauf, M. Fahnle, T. Roth, M. Cinchetti, and M. Aeschlimann, Nat. Mater. **9**, 259 (2010).

[8] L. Guidoni, E. Beaurepaire, and J. Y. Bigot, Phys. Rev. Lett. **89**, 017401 (2002).

[9] K. Carva, M. Battiato, D. Legut, and P. M. Oppeneer, Phys. Rev. B **87**, 184425 (2013).

[10] M. Battiato, K. Carva, and P. M. Oppeneer, Phys. Rev. Lett. **105**, 027203 (2010).

[11] M. Battiato, K. Carva, and P. M. Oppeneer, Phys. Rev. B **86**, 024404 (2012).

[12] V. Shokeen, M. Sanchez Piaia, J.-Y. Bigot, T. Muller, P. Elliott, J. K. Dewhurst, S. Sharma, and E. K. U. Gross, Phys. Rev. Lett. **119**, 107203 (2017).

[13] J. Y. Bigot, M. Vomir, L. H. F. Andrade, and E. Beaurepaire, Chem. Phys. **318**, 137 (2005).

[14] D. A. Garanin, Phys. A **172**, 470 (1991).

[15] J. H. Mentink, J. Hellsvik, D. V. Afanasiev, B. A. Ivanov, A. Kirilyuk, A. V. Kimel, O. Eriksson, M. I. Katsnelson, and Th. Rasing, Phys. Rev. Lett. **108**, 057202 (2012).

[16] C. Stamm, T. Kachel, N. Pontius, R. Mitzner, T. Quast, K. Holldack, S. Khan, C. Lupulescu, E. F. Aziz, M. Wietstruk, H. A. Dürr, and W. Eberhardt, Nat. Mater. **6**, 740 (2007).

[17] I. Radu, G. Woltersdorf, M. Kiessling, A. Melnikov, U. Bovensiepen, J. U. Thiele, and C. H. Back, Phys. Rev. Lett. **102**, 117201 (2009).

[18] I. Radu, K. Vahaplar, C. Stamm, T. Kachel, N. Pontius, H. A. Durr, T. A. Ostler, J. Barker, R. F. L. Evans, R. W. Chantrell, A. Tsukamoto, A. Itoh, A. Kirilyuk, Th. Rasing, and A. V. Kimel, Nature (London) **472**, 205 (2011).

[19] C. Boeglin, E. Beaurepaire, V. Halté, V. Lopez-Flores, C. Stamm, N. Pontius, H. A. Durr, and J. Y. Bigot, Nature (London) **465**, 458 (2010).

[20] N. Bergeard, V. Lopez-Flores, V. Halte, M. Hehn, C. Stamm, N. Pontius, E. Beaurepaire, and C. Boeglin, Nat. Commun. **5**, 3466 (2014).

[21] C. La-O-Vorakiat, M. Siemens, M. M. Murnane, H. C. Kapteyn, S. Mathias, M. Aeschlimann, P. Grychtol, R. Adam, C. M. Schneider, J. M. Shaw, H. Nembach, and T. J. Silva, Phys. Rev. Lett. **103**, 257402 (2009).

[22] C. La-O-Vorakiat, E. Turgut, C. A. Teale, H. C. Kapteyn, M. M. Murnane, S. Mathias, M. Aeschlimann, C. M. Schneider, J. M. Shaw, H. T. Nembach, and T. J. Silva, Phys. Rev. X **2**, 011005 (2012).

[23] S. Valencia, A. Kleibert, A. Gaupp, J. Rusz, D. Legut, J. Bansmann, W. Gudat, and P. M. Oppeneer, Phys. Rev. Lett. **104**, 187401 (2010).

[24] S. Mathias, C. La-O-Vorakiat, P. Grychtol, P. Granitzka, E. Turgut, J. M. Shaw, R. Adam, H. T. Nembach, M. E. Siemens, S. Eich, C. M. Schneider, T. J. Silva, M. Aeschlimann, M. M. Murnane, and H. C. Kapteyn, Proc. Natl. Acad. Sci. USA **109**, 4792 (2012).

[25] S. Günther, C. Spezzani, R. Ciprian, C. Grazioli, B. Ressel, M. Coreno, L. Poletto, P. Miotti, M. Sacchi, G. Panaccione, V. Uhlíř, E. E. Fullerton, G. De Ninno, and C. H. Back, Phys. Rev. B **90**, 180407(R) (2014).

[26] M. Hofherr *et al.*, Phys. Rev. B **98**, 174419 (2018).

[27] S. G. Gang, R. Adam, M. Plotzing, M. von Witzleben, C. Weier, U. Parlak, D. E. Burgler, C. M. Schneider, J. Rusz, P. Maldonado, and P. M. Oppeneer, Phys. Rev. B **97**, 064412 (2018).

[28] M. Hofherr, S. Häuser, J. K. Dewhurst, P. Tengdin, S. Sakshath, H. T. Nembach, S. T. Weber, J. M. Shaw, T. J. Silva, H. C. Kapteyn, M. Cinchetti, B. Rethfeld, M. M. Murnane, D. Steil, B. Stadtmüller, S. Sharma, M. Aeschlimann, and S. Mathias, Sci. Adv. **6**, eaay8717 (2020).

[29] F. Willems, C. von Korff Schmising, C. Strüber, D. Schick, D. W. Engel, J. K. Dewhurst, P. Elliott, S. Sharma, and S. Eisebitt, Nat. Commun. **11**, 871 (2020).

[30] R. Carley, K. Dobrich, B. Frietsch, C. Gahl, M. Teichmann, O. Schwarzkopf, P. Wernet, and M. Weinelt, Phys. Rev. Lett. **109**, 057401 (2012).

[31] I. Radu, C. Stamm, A. Eschenlohr, F. Radu, R. Abrudan, K. Vahaplar, T. Kachel, N. Pontius, R. Mitzner, K. Holldack, A. Föhlisch, T. A. Ostler, J. H. Mentink, R. F. L. Evans, R. W. Chantrell, A. Tsukamoto, A. Itoh, A. Kirilyuk, A. V. Kimel, and Th. Rasing, SPIN **5**, 1550004 (2015).

[32] D. Hinzke, U. Atxitia, K. Carva, P. Nieves, O. Chubykalo-Fesenko, P. M. Oppeneer, and U. Nowak, Phys. Rev. B **92**, 054412 (2015).

[33] S. Mukhopadhyay, S. Majumder, S. N. Panda, and A. Barman, Nanotechnology **34**, 235702 (2023).

[34] U. Atxitia, P. Nieves, and O. Chubykalo-Fesenko, Phys. Rev. B **86**, 104414 (2012).

[35] U. Atxitia and O. Chubykalo-Fesenko, Phys. Rev. B **84**, 144414 (2011).

[36] A. J. Schellekens and B. Koopmans, Phys. Rev. B **87**, 020407(R) (2013).

[37] S. Wienholdt, D. Hinzke, K. Carva, P. M. Oppeneer, and U. Nowak, Phys. Rev. B **88**, 020406(R) (2013).

[38] P. Nieves, D. Serantes, U. Atxitia, and O. Chubykalo-Fesenko, Phys. Rev. B **90**, 104428 (2014).

[39] J. Walowski, G. Müller, M. Djordjevic, M. Münzenberg, M. Kläui, C. A. F. Vaz, and J. A. C. Bland, Phys. Rev. Lett. **101**, 237401 (2008).

[40] F. Schlickeiser, U. Atxitia, S. Wienholdt, D. Hinzke, O. Chubykalo-Fesenko, and U. Nowak, Phys. Rev. B **86**, 214416 (2012).

[41] A. Gurevich and G. A. Melkov, *Magnetization Oscillations and Waves* (CRC Press, London, 1996), doi:10.1201/9780138748487.